

# LPP EUV Source Development for HVM

Björn A. M. Hansson\*, Igor V. Fomenkov, Norbert R. Böwering, Alex I. Ershov, William N. Partlo, David W. Myers, Oleh V. Khodykin, Alexander N. Bykanov, Curtis L. Rettig, Jerzy R. Hoffman, Ernesto Vargas L, Rod D. Simmons, Juan A. Chavez, William F. Marx, and David C. Brandt  
Cymer Inc, San Diego, CA 92127, USA

## ABSTRACT

This paper provides a detailed review of development progress for a laser-produced-plasma (LPP) extreme-ultra-violet (EUV) source with performance goals targeted to meet joint requirements from all leading scanner manufacturers. We present the latest results on drive laser power and efficiency, source fuel, conversion efficiency, debris mitigation techniques, multi-layer-mirror coatings, collector efficiency, intermediate-focus (IF) metrology, mass-limited droplet generation, laser-to-droplet targeting control, and system use and experience. Results from several full-scale prototype systems are discussed. In addition, a multitude of smaller lab-scale experimental systems have also been constructed and tested. This paper reviews the latest experimental results obtained on these systems with a focus on the topics most critical for an HVM source. Laser produced plasma systems have been researched as probable light source candidates for an EUV scanner for optical imaging of circuit features at 32nm and beyond nodes on the ITRS roadmap. LPP systems have inherent advantages over alternative source types, such as Discharge Produced Plasma (DPP), with respect to power scalability, etendue, collector efficiency, and component lifetime. The capability to scale LPP power with repetition rate and modular design is shown. A path to meet requirements for production scanners planned well into the next decade is presented. This paper includes current testing results using a 320mm diameter near-normal-incidence elliptical collector, the first to be tested in a full-scale LPP system. With the collector in-situ, intermediate focus (IF) metrology capability is enabled, and data is presented that describes the quality of light at IF.

**Keywords:** EUV source, EUV lithography, Laser Produced Plasma, High Volume Manufacturing

## 1. INTRODUCTION

EUV Lithography is currently slated as the next critical dimension imaging solution after 193nm immersion lithography below the 32nm node on the International Technology Roadmap for Semiconductors (ITRS) beginning in 2013. The availability of a high power source for 13.5 nm radiation has been categorized as high risk and ranked with other technologies requiring significant development to enable the realization of EUV lithography. The top risk technology continues to be the photoresist with the sensitivity and line-edge-roughness (LER) performance parameters needing the greatest amount of development. Photoresist sensitivity and other light absorbing materials are used to derive EUV source power requirements within the usable bandwidth (BW) of 2%. A value of 5 mJ/cm<sup>2</sup> for the photoresist requires and EUV power of >115W 2%BW at the intermediate focus (IF) to enable >100wph scanner throughput, and 10mJ/cm<sup>2</sup> requires >180W 2%BW at IF. Photoresist sensitivities above 20mJ/cm<sup>2</sup> could drive power requirements well above 200W. Therefore, a scalable EUV source is necessary to enable the evolution of EUV lithography during the life cycle of the technology. Low power Discharge-Produced-Plasma (DPP) sources have been shown to be capable of producing from 10 to 35W at IF but are not expected to be scalable beyond 50 to 100W. Laser-Produced-Plasma sources, on the other hand, are expected to deliver the necessary power for critical-dimension high-volume manufacturing (HVM) scanners for the production of integrated circuits in the post 193nm immersion era.

LPP EUV lithography light sources generate the required 13.5nm radiation by depositing laser energy into a source element, such as xenon (Xe), tin (Sn) or lithium (Li); producing highly ionized plasma with electron temperatures of several 10's of eV. The energetic radiation created by the recombination and de-excitation of these ions is emitted into all directions, is collected by a normal incidence mirror (collector), and focused to an intermediate point from where it is relayed to the scanner optics and ultimately to the wafer. Conversion efficiency (CE) of the laser energy into EUV energy is critical to meeting the required powers. Several combinations of laser wavelength and source element CE are

---

\* bhansson@cymer.com

discussed in the present paper. The normal incidence mirror is protected from the plasma with debris mitigation technology. High-energy ions, fast neutrals, and residual source element particles are mitigated to maintain the reflectivity of the collector mirror and enable long component lifetime. Metrology to measure the properties of light at both the plasma and IF are used to qualify the performance of the source. IF metrology is introduced to accurately measure 2%BW and assess the angular distribution of EUV energy behind the intermediate focus.

## 2. LPP SYSTEM PROTOTYPE

The latest version of our previously presented family of LPP system prototypes<sup>1</sup> has been significantly upgraded. Several important experimental results have been obtained over the last 12 months. Figure 1 shows a photograph of the latest system.

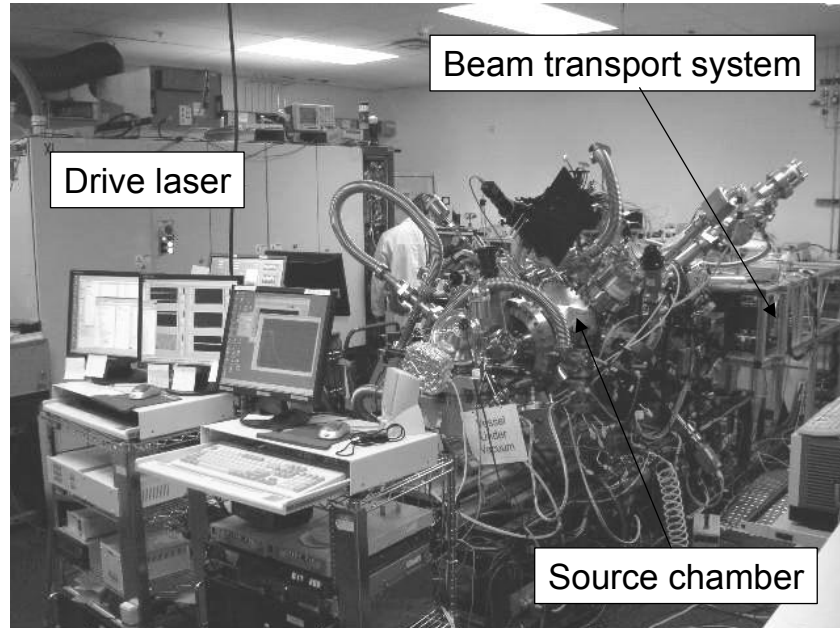


Figure 1: The latest LPP system prototype.

As previously described it consists of an 800W, 4kHz, XeF drive laser based on Cymer's standard ArF deep ultraviolet (DUV) production lasers. It has a laser beam transport system responsible to deliver and focus the laser beam onto the target in the source chamber. The source chamber is an ultra-high vacuum (UHV) chamber containing a target delivery system generating tin droplets of diameter  $< 100 \mu\text{m}$ . The system is equipped with control software and hardware that can place the target droplets at a given position in space to within a few  $\mu\text{m}$  and also control the laser beam transport system such that the droplets are targeted with a similar accuracy of only a few  $\mu\text{m}$ . Furthermore, the system is equipped with a full suite of at-plasma metrology systems such as EUV spectrometer, EUV pinhole camera, EUV energy monitors, ion energy monitors. The most important upgrade of the prototype family since last described is the introduction of a large near-normal-incidence collector to the system. Figure 2 is a photograph of the collector during installation in the system prototype where one of two protective doors is being attached.

This collector subsystem is described in detail in a separate paper in these proceedings<sup>2</sup>. Briefly, it is a sub-aperture configuration with half the diameter of an HVM, 5sr 600 mm diameter collector but with the same elliptical curvature. This results in a light collection solid angle of 1.6 sr. The collector furthermore has a multilayer coating capable of operating at temperatures up to  $500 \text{ }^\circ\text{C}$  in order to be compatible with the previously described technique to evaporate Li from the collector surface<sup>1</sup>. At the time of the introduction of the collector, the source system has been equipped with a full suite of metrology tools for source diagnostics after the IF. This will be discussed in more details in next section as well as the debris mitigation systems implemented to increase the lifetime of the collector.

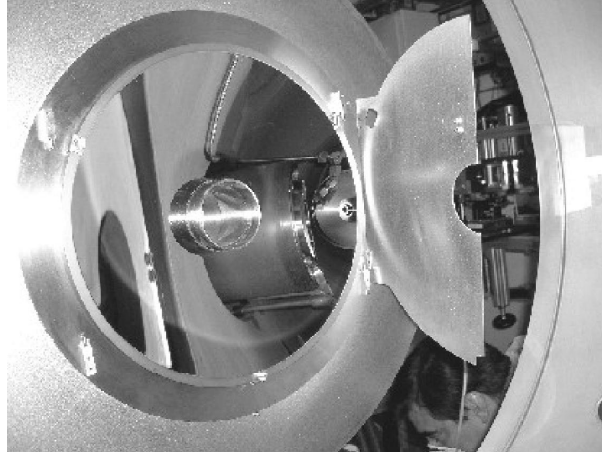


Figure 2: The 1.6 sr, 300 mm diameter collector during installation in the latest LPP system prototype. One of two protective doors is being attached.

### 3. LPP PROTOTYPE PERFORMANCE

The typical CE obtained with the system is  $\sim 0.5\%$  into 2%BW and  $2\pi$ sr. This CE may seem low compared to the high CE numbers of about 5% that have been published using tin as target material.<sup>3</sup> However, tin together with short wavelength radiation, such as  $\lambda=351$  nm in this case, does not result in high CE values as supported by simulations discussed later in this paper (see Figure 12). Similar results have been reported for tin doped droplet targets when illuminated with the third harmonic YAG at  $\lambda=355$  nm rather than the fundamental YAG at  $\lambda=1064$  nm.<sup>4</sup> Using lithium as target material or a longer wavelength laser would certainly result in higher CE and power. However, the combination tin and XeF is very convenient for system development experiments due to the availability of the high power XeF laser and the less problematic operation of tin compared to lithium when, e.g., the vacuum chamber has to be vented to atmosphere at regular intervals.

With the collector installed, it was for the first time possible to measure the average usable EUV power after the IF instead of just pulse-to-pulse EUV energy measured at the plasma. An arrangement for EUV power measurements is illustrated in Figure 3.

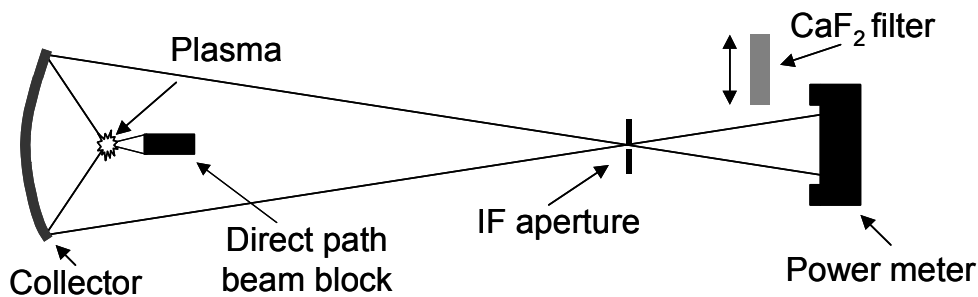


Figure 3: Experimental arrangement to measure the total power transmitted through the IF aperture. The EUV is determined by subtracting the out-of-band power measured with a CaF<sub>2</sub> filter in the optical path from the total power measured.

The detector is a calorimetric laser power meter head converted for in-vacuum operation. Its detection surface covers the full cone of radiation after the IF. All radiation reflected by the collector and transmitted through the IF aperture is detected by the power meter. Since the collector not only reflects EUV radiation, but also DUV, visible and infra-red (IR) radiation this out-of-band component must be subtracted from the total signal in order to obtain only the EUV portion. The out-of-band portion of the radiation is determined by inserting a CaF<sub>2</sub> plate in the beam path and registering the power level. The measured total EUV power after the IF was 0.5W after subtraction of the out-of-band portion that amounted to 15% of the total power. By this method the total EUV radiation around 13.5 nm that is reflected by the

collector with a bandwidth of ~4% is measured. In order to detect only the portion that is radiated into 2% bandwidth, an arrangement with two multilayer mirrors whose combined reflectivity curves yield exactly 2% bandwidth has been used, as illustrated in Figure 4. The result obtained with this measurement setup correlates well with the total EUV measurements described above as well as with the pulse-to-pulse EUV energy measurements obtained directly at the plasma, verifying the accuracy of the models previously used to estimate the system's total 2%-in-band power.

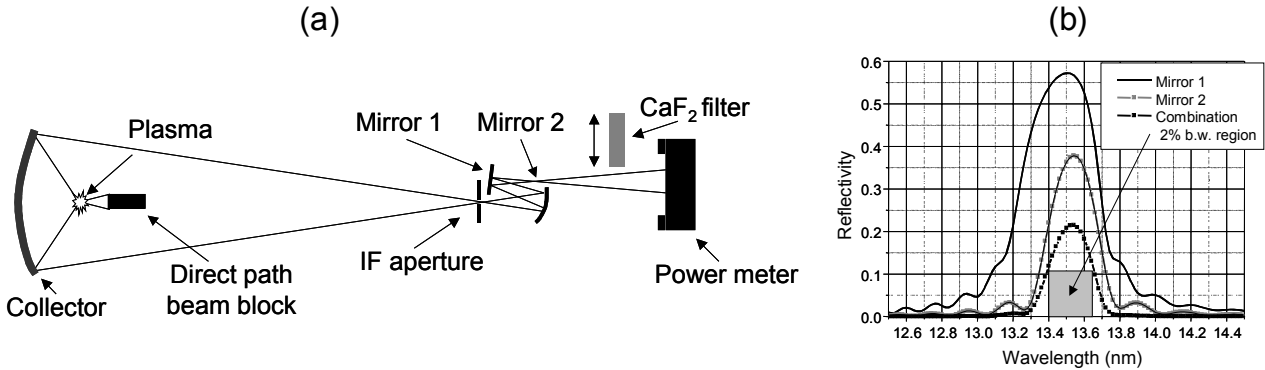


Figure 4: The experimental arrangement (a) to measure only the 2% in-band radiation around 13.5 nm through the combined reflectivity of mirror 1 and 2 (b).

In addition, using the configuration illustrated in Figure 5, the angular emission distribution after the IF can be measured. A fluorescence plate made of Ce:YAG with a Zr/Si coating of 150nm/50nm is placed after the IF. The Zr/Si coating transmits only EUV light, blocking the visible and DUV radiation that is also reflected by the collector. The EUV radiation incident on the Ce:YAG plate causes fluorescence creating an image of the EUV intensity distribution over its surface. A conventional CCD camera can detect this fluorescence to record the angular emission intensity distribution after the IF. Figure 6b illustrates a typical fluorescent converter image as well as the horizontal intensity cross section with the plasma well aligned to the collector and the laser beam aligned to the droplets.

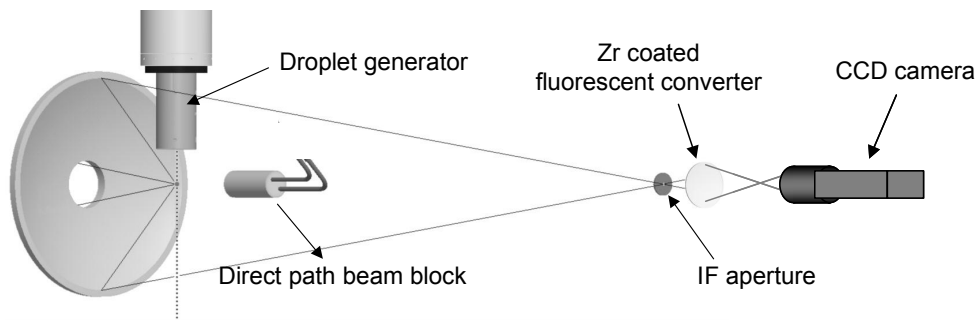


Figure 5: The experimental arrangement to measure the angular emission distribution after the IF aperture by imaging the EUV induced fluorescence in a Ce:YAG plate with a standard CCD camera.

The central aperture in the collector through which the laser is focused as well as the shadow of the droplet generator and the mounting structure for the beam stop blocking the direct beam path are all visible in the image. This technique can detect both variations in the angular emission from the plasma as well as reflectivity variations over the surface of the collector. In Figure 6, e.g., a few small spots with lower reflectivity on the mirror are visible at a location of about 7 o'clock. The dark spot just below the central aperture is due to an absorbing contamination on the coated surface of the fluorescent converter. The general intensity distribution with higher intensity towards the center of the image is not caused by non-uniform emission from the plasma, but corresponds well to simulated results assuming uniform angular emission distribution from the plasma itself. Apart from measuring the intrinsic intensity distribution at best alignment, we can also deliberately misalign the laser to the droplets. Figure 6a and Figure 6c illustrate how the emission distribution is shifted from the left to the right as the laser droplet interaction alignment is deliberately shifted.

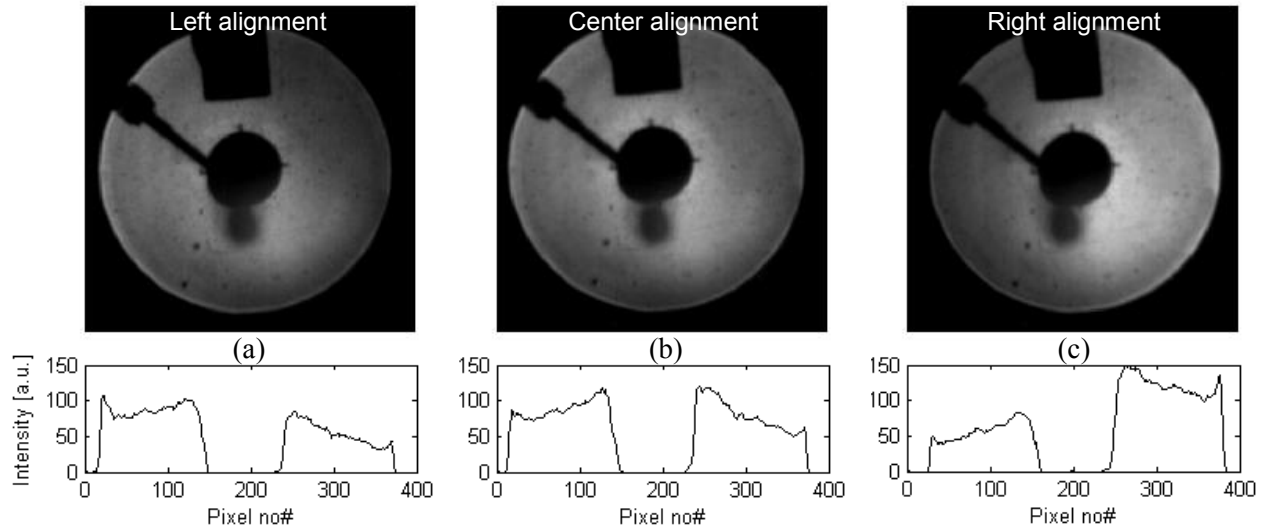


Figure 6: Fluorescent converter image as well as the horizontal intensity cross section with the plasma well aligned to the collector and the laser beam hitting the center of the droplets (b) as well as images and intensities resulting from deliberate targeting

Apart from measuring the source performance after the IF we continue the source characterization with measurements taken directly at the plasma. As an example, pulse-to-pulse energy measurements are currently obtained by averaging the signal of 4 different EUV sensors directed at the plasma from 4 different orthogonal directions. The pulse-to-pulse energy stability was measured and the 100-running-average dose stability calculated as illustrated in Figure 7a resulting in a dose stability of 0.83% ( $1\sigma$ ) and a pulse-to-pulse stability of 6.0% ( $1\sigma$ ). However, the dose stability can be significantly improved by using closed-energy-loop control as illustrated in Figure 7b leading to a dose stability of 0.17% ( $1\sigma$ ) and a shot-to-shot stability of 7.8% ( $1\sigma$ ).

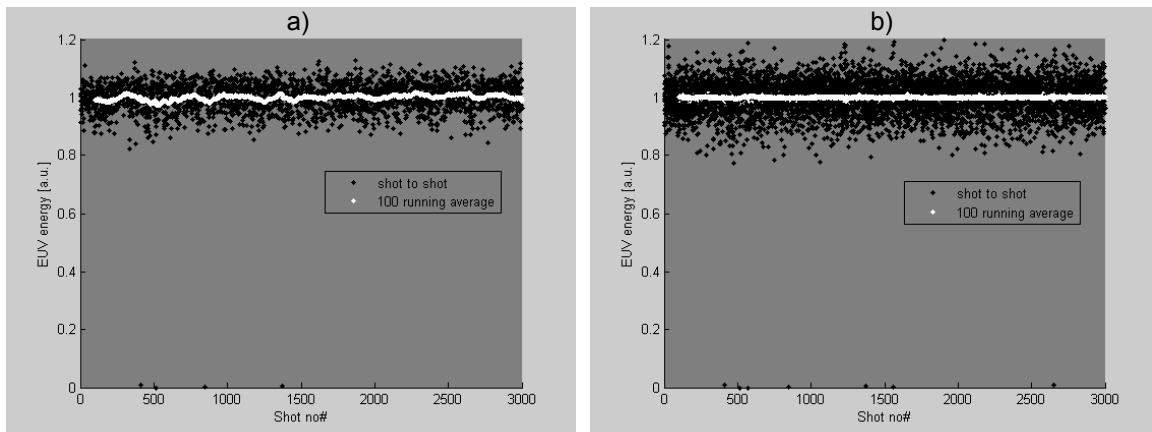


Figure 7: Pulse-to-pulse energy stability and 100-running-average dose stability running open loop (a) and closed loop (b)

#### 4. MIRROR LIFETIME EXPERIMENTS

Before installing the collector in our source prototype we did several mirror lifetime related experiments. Initially we examined where the bulk of the tin debris from a targeted droplet would be directed after a plasma event. Figure 8 is an image taken  $9\mu\text{s}$  after the plasma event clearly illustrating how the majority of the target material is ejected in the same direction as laser pulse, i.e., away from the collector in our geometry.

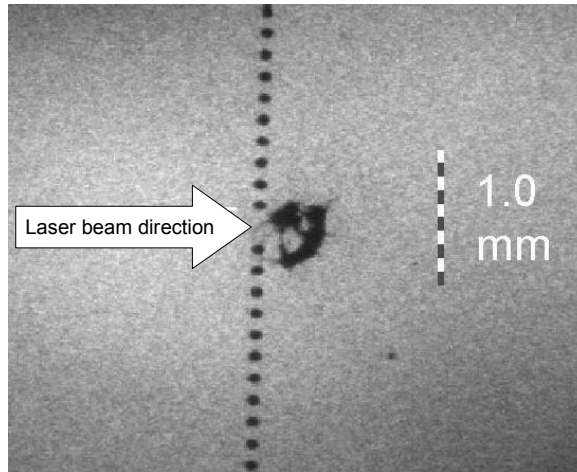


Figure 8: Image taken  $9\mu\text{s}$  after the plasma event clearly illustrating how the bulk of the target material is ejected in the direction of the laser pulse, i.e., away from the collector in our geometry.

However, not all material will be emitted away from the collector. It is well known that high-energy ions are ejected towards the direction of the incident laser pulse. In order to investigate the ion flux in our specific system prototype, a Faraday cup was mounted close to where the collector is normally. As illustrated by the dashed line in Figure 9, the bulk of the ions in the baseline case have an energy about 2 keV. We also applied one of our previously reported<sup>1</sup> debris mitigation techniques and as expected measured a 100-fold reduction of the ion flux as illustrated by the solid line.

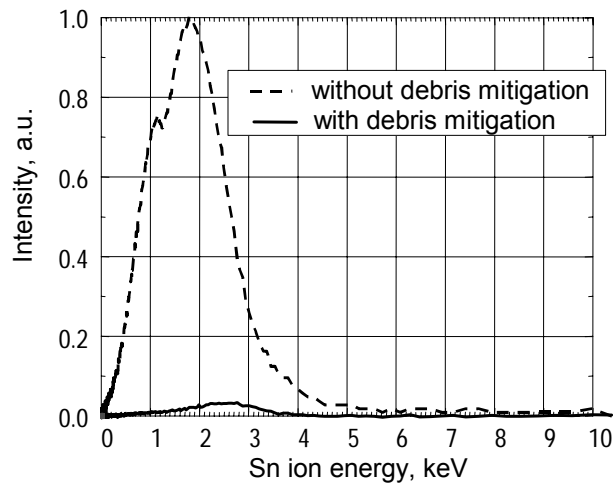


Figure 9: Ion energies with and without debris mitigation obtained with a Faraday cup placed in the same direction as where the collector sits if installed.

The most comprehensive test for determination of the potential lifetime of the collector was carried out in an experiment exposing actual mirror samples. Silicon witness plates coated with the same high-temperature compatible multilayer as used for the actual collector were mounted at positions corresponding exactly to the location of the surface of the collector. Using only one debris mitigation technique the samples were exposed to 45 million pulses of tin LPP. A comparison of the EUV reflectance measured with synchrotron radiation for a reference sample and for the exposed sample indicated that no reduction in reflectivity took place. Furthermore, some of the samples were coated with only eight layer periods of the high-temperature MLM coating and the capping layer to facilitate layer counting. Data obtained with SIMS analysis are shown in Figure 10. In contrast to the more complex evolution of the relative height of the sputter peaks, the sputter depth can be readily used for quantitative analysis if the layer number is not too high. The data indicates that after 45 million pulses only one SIMS peak is missing and at least 7 periods of the multilayer are still remaining on the sample. Using this result as a basis for the layer erosion estimates and carrying out calculations of the

multilayer reflectivity, we conclude that the expected mirror lifetime (corresponding to a reflectivity drop by 10 %) is in excess of 2 billion pulses. When combining the employed debris mitigation technique with an additional mitigation method or with sacrificial MLM layers a lifetime on the order of at least 45 billion pulses is projected. These encouraging results support that tin can be used as target material for an HVM LPP source in addition to lithium as reported previously.<sup>1</sup>

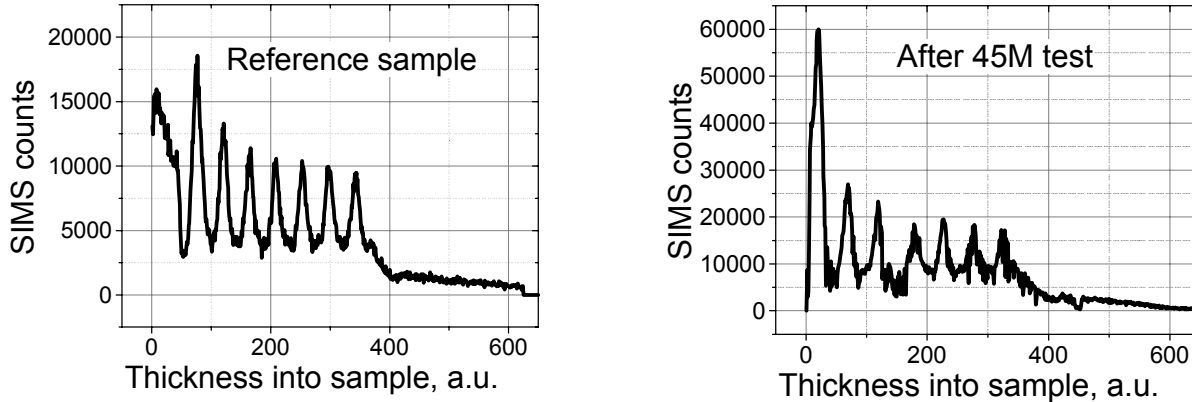


Figure 10: SIMS measurement result for sputtering multilayer material, counts as function of sputter depth. The reference sample shows 8 sputter peaks whereas the exposed sample shows 7.

### 5. ROADMAP AND HVM OPTIONS

As already discussed in a previous paper<sup>1</sup> the history of DUV photolithography shows that the power required from the laser source did not decrease over time. On the contrary, from the time DUV Excimer lasers were first used in a production environment, the power requirements actually increased six times. Correspondingly, we believe that a viable EUV source technology must take into account that the power requirements for the ultimate EUV sources will likely increase over time, as illustrated in the EUV source performance roadmap of Table 1.

LPP EUV Source Performance Roadmap			
	Gen 1	Gen 2	Gen 3
Total Rep Rate (kHz)	48	60	72
<b>Laser power (kW)</b>	<b>9.6</b>	<b>12.0</b>	<b>14.4</b>
In-band CE	3.5%	4.0%	4.5%
Geometric collection efficiency (sr)	5	5	5.5
Collector average reflectivity	50%	50%	50%
Optical transmission	80%	82%	84%
<b>Total power at IF (W)</b>	<b>110</b>	<b>155</b>	<b>230</b>

Table 1: Roadmap supporting increased EUV power through mainly increased drive laser power.

As is evident from the table, a high CE solution is necessary in order to limit drive laser powers and, in this way, also the cost of the system. As previously discussed we currently see two potential plasma-target-material solutions, namely the use of lithium or tin, that can both support high CE as well as the required collector lifetime.

Figure 11 plots laboratory measurements of lithium CE as a function of intensity for 5 different drive laser wavelengths. On the right side of the figure is a comparison of these measurements to modeling results. The general shape shows good agreement between modeled and measured CE vs. wavelength with the absolute measurements slightly exceeding the model calculations. Even under these non-optimized conditions the lithium CE is high, approaching 3%, and it is relatively insensitive to laser wavelengths in the range from 266nm to 1.064µm. Specifically, this would allow for use of the efficient drive laser solution based on XeF Excimer amplifiers seeded by a Nd:YLF master oscillator as is described in another paper in these proceedings.<sup>5</sup>

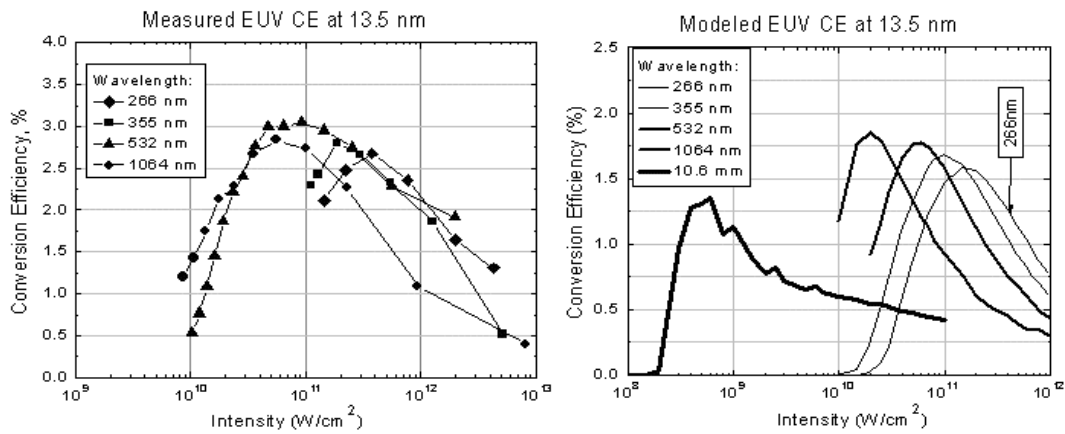


Figure 11: Lithium CE measurements and model projections vs. wavelength.

Figure 12 plots measurements of tin CE as a function of intensity for several drive laser wavelengths as well as modeling results. In this case there is also a good correspondence observed for the model of Figure 12a that longer laser wavelength yield higher CE with the measured CE of ~2% for a solid state YAG laser at 1064 nm laser wavelength and ~4% for a CO<sub>2</sub> laser at 10.6 μm. In addition, CE as high as 5%, has been reported for 1064 nm wavelength elsewhere.<sup>3</sup> Based on these results, tin LPP sources based on either solid state YAG or CO<sub>2</sub> lasers appear to be viable options for an HVM source. Results on the feasibility of a high-power, short-pulse-length CO<sub>2</sub> laser is reported in another paper in these proceedings.<sup>5</sup>

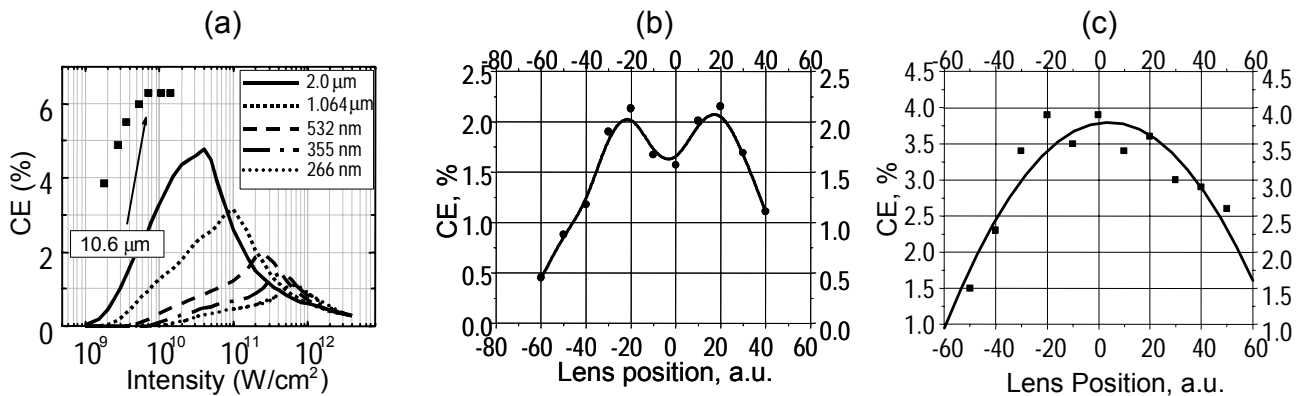


Figure 12: Tin CE vs. laser wavelength model projections (a) and CE measurements for 1064 nm (b) and 10.6 μm (c) laser wavelengths.

Apart from differences in CE there are other aspects that will determine what target material is most feasible for a HVM EUV source. As an example, Figure 13 illustrates how Li-ion energies are about a factor of 5 lower than Sn-ion energies. The lower ion energies together with the generally lower sputter yield for Li compared to Sn is expected to result in MLM sputtering for Li that is reduced by an order of magnitude compared to Sn. In addition, as discussed in a previous paper<sup>1</sup>, the Li line spectrum is significantly narrower than the multi-line Sn emission spectrum, supporting more variation in the central wavelength for the numerous mirrors within the scanner's optical system without additional loss of transmitted EUV power to the wafer. Measurements comparing the spectral output from Sn and Li in the EUV range and the ultraviolet-visible band from 200 to 800nm also show that lithium has much lower integrated spectral output in these bands, possibly eliminating the need for spectral purity filters.

Ultimately, the most feasible and cost effective LPP technology solution will be chosen for an HVM EUV source. Currently it appears that it will be based on either an excimer laser with a Li target, a solid state laser with a Sn or Li target, or a CO<sub>2</sub> laser with a Sn target.

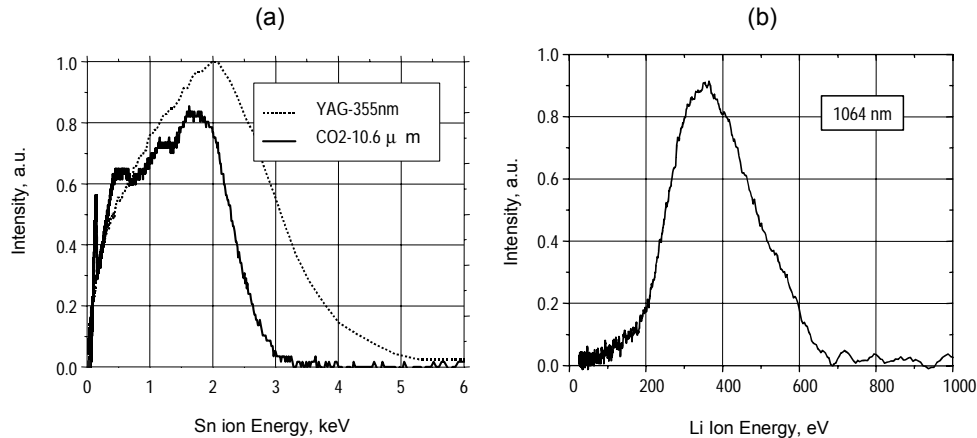


Figure 13: Typical ion energies measured with a Faraday cup for tin (a) and lithium (b).

## 6. SUMMARY

Laser-produced plasma has been shown to be a viable source technology with scalability to meet requirements from leading scanner manufacturers and provide a path toward higher power as the lithography tools evolve over their life cycle. A sub-aperture 320mm diameter high-temperature graded multi-layer-coated near-normal-incidence collector has been developed and installed into our prototype system enabling the measurement of EUV photons at IF for the first time. Measured power and stability have been reported. Images of the angular distribution of EUV energy at IF have been reported. Intermediate focus metrology has been developed and put into use to measure accurate 2% bandwidth in-band data at the IF. Experiments using coated witness samples have been performed to estimate the lifetime of the collector coating and have shown feasibility to reach 45 billion pulses. High-conversion-efficiency combinations of laser wavelength and source element have been reported well in excess of 2% CE. Our debris mitigation technology has been shown to be successful with Sn and Li enabling them as alternatives to Xe. High CE values allow the roadmap of laser power to remain well below the expected power needed from a Xe LPP source and provide low cost solutions to meet the needs of chipmakers. EUV lithography is expected to be the critical dimension imaging solution post 193nm immersion in 2013. LPP source technology is the most viable solution to enable the IF power requirement projected in the future and to provide the much needed margin in photoresist sensitivity, optics degradation, process latitude, and overall equipment throughput.

## ACKNOWLEDGEMENTS

The authors gratefully acknowledge the valuable contributions from Martin J. Neumann, Matthew R. Hendricks, Huatan Qiu, Eithan Ritz, Reece A. DeFrees, Darren A. Alman, Erik L. Antonsen, Brian E. Jurczyk and David N. Ruzic of University of Illinois – Urbana Champaign, Sergiy Yulin, Nicolas Benoit, Torsten Feigl and Norbert Kaiser of Fraunhofer Institut f. Angewandte Optik und Feinmechanik, Joseph J. MacFarlane and Igor Golovkin of Prism Computational Sciences, Eric Gullikson and Franklin Dollar of Lawrence Berkeley National Laboratory and Martin Richardson of University of Central Florida.

## REFERENCES

- <sup>1</sup> D. W. Myers, I. V. Fomenkov, B. A. M. Hansson, B. C. Klene, D. C. Brandt, in: *Proc. of SPIE Vol. 5751, Emerging Lithographic Technologies IX*, R. S. Mackay, Ed., 248-259 (2005).
- <sup>2</sup> Norbert R. Böwering, Alex I. Ershov, William F. Marx, Oleh V. Khodykin, Björn A. M. Hansson, Ernesto Vargas L., Juan A. Chavez, Igor V. Fomenkov, Dave W. Myers, David C. Brandt, "EUV Source Collector" *In these Proceedings of SPIE Vol. 6151, Emerging Lithographic Technologies X*, (2006)

<sup>3</sup> Chiew-Seng Koay, Simi George, Kazutoshi Takenoshita, Robert Bernath, Etsuo Fujiwara, Martin Richardson, Vivek Bakshi *Proc. SPIE Vol. 5751* 279-292 (2005)

<sup>4</sup> Martin Richardson, Chiew-Seng Koay, Kazutoshi Takenoshita, Simi George, Tobias Schmid, Robert Bernath, Somsak Teerawattansook, Greg Shimkaveg, William T. Silfvast, “The Tin-Doped Droplet Laser Plasma Source – Meeting Roadmap Requirements” *Proc. Int. Sematech EUVL Symposium, San Diego (2005)*.

<sup>5</sup> Igor V. Fomenkov, Björn A.M. Hansson, Norbert R. Böwering, Alex I. Ershov, William N. Partlo, Vladimir B. Fleurov, Oleh V. Khodykin, Alexander N. Bykanov, Curtis L. Rettig, Jerzy R. Hoffman, Ernesto Vargas L., Juan A. Chavez, William F. Marx, David C. Brandt, “High Power Low Cost Drive Laser for LPP Source” *In these Proceedings of SPIE Vol. 6151, Emerging Lithographic Technologies X*, (2006)